Nematics with dispersed polymer fibrils: A Monte Carlo study of the external-field-induced switching

C. Chiccoli,[1] P. Pasini,[1] G. Skačej,[2] C. Zannoni,[3] and S. Žumer[2]

[1]*INFN, Sezione di Bologna, Via Irnerio 46, I-40126 Bologna, Italy*
[2]*Oddelek za fiziko, Univerza v Ljubljani, Jadranska 19, SI-1000 Ljubljana, Slovenia*
[3]*Dipartmento di Chimica Fisica ed Inorganica and INSTM, Università, Viale Risorgimento 4, I-40136 Bologna, Italy*

We present a Monte Carlo study of molecular ordering in nematics with dispersed regular and random arrays of straight and distorted polymer fibrils. We focus on the collective molecular reorientation—the switching—resulting from the competing aligning effects of fibrils and of a progressively applied transversal external field, and for straight fibrils identify stuctural Fréedericksz and saturation transitions. The role of fibril topography in the switching is monitored by simulating electric capacitance Slightly distorted fibrils are shown to give a sharper switching at a lower threshold.

Interest in soft matter physics is shifting to complex systems of biological nature or created artificially. Fascinating examples—challenging both from the technological and fundamental point of view—are offered by nanoscale and mesoscale composites, where liquid crystals (LC) interact with random or regular perturbers [1–3]. Such perturbers consist, e.g., of thin (even nanometric) polymer fibrils obtained by polymerization of monomers dissolved in LC that can either memorize the order of the host LC phase [3] or follow a regular pattern as defined in a lithographic formation process [4]. The fiber topography depends sensitively on the polymerization conditions, such as temperature, curing light wavelength and intensity, or monomer solubility [5]. Because of their high surface-to-volume ratio the polymer fibrils influence orientational ordering of the surrounding liquid crystal even at low polymer concentrations [3,6–8]. The actual ordering is affected by the competition between effects of the fiber network (anchoring), temperature, and external fields. Apart from exhibiting a variety of confinement-related phenomena, such composite materials are promising for the construction of electro-optical devices, based on the "switching" phenomenon. This consists of a reorganization of the nematic director—initially aligned by the polymer network—by applying an external electric field producing changes in electric capacitance, optical transmission, light scattering, etc. [3,6–8]. Thus, studies of formation and properties of liquid crystal-dispersed network systems (LCDNS) are very timely, also for the next generation of LC displays [4,6]. In the past, there have been several (mostly experimental) studies devoted to LCDNS [6–8]. So far the effect of such complex confinement was described phenomenologically [6–8], while at the molecular level (facilitating studies of any nontrivial sample geometry) only a regular fiber array in absence of external fields was treated [9]. In this paper, we investigate the field-induced switching in LCDNS by means of Monte Carlo (MC) simulations, starting from a simple pairwise potential and giving great emphasis to the role of polymer network topography.

Our simulations are based on the Lebwohl-Lasher (LL) model [10] in which uniaxial nematic molecules (or close-packed clusters containing up to 10^2 molecules [11]) are represented by unit vectors ("particles") $\mathbf{u}_i$. The LL model, despite having particles fixed onto sites of a cubic lattice (with spacing a, 1 nm$\lesssim a \lesssim 5$ nm), reproduces the orientational behavior of nematics sufficiently well [11]. We model the effect of an external field by adding a quadratic contribution to the standard N-particle LL Hamiltonian [11]:

$$U_N = -\sum_{\langle i<j \rangle} \epsilon_{ij} P_2(\mathbf{u}_i \cdot \mathbf{u}_j) - \epsilon \eta \sum_{i=1}^{N} P_2(\mathbf{f} \cdot \mathbf{u}_i). \quad (1)$$

Here, $P_2(x) = \frac{1}{2}(3x^2-1)$, $\mathbf{f}$ stands for a unit vector oriented along the external field $\mathbf{H}$ ($\mathbf{H} = H\mathbf{f}$), and ϵ_{ij} is a positive constant, nonzero only for nearest-neighbor particles: ϵ for nematic-nematic interactions and $w\epsilon$ for nematic-polymer interactions (also included in the first sum). Moreover, dimensionless $\eta \propto H^2$ gives the strength of the field coupling. Here, $\mathbf{H}$ was assumed homogeneous throughout the sample despite the (possibly strong) inhomogeneity of the nematic. In practice, $\mathbf{H}$ can be either an electric or magnetic field [12], but the homogeneity approximation is reasonable in the magnetic case only.

As a first step towards modeling the topography of the polymer network, we considered a single straight cylindrical fiber oriented along the z axis by defining a "jagged" cylinder comprising all the particles lying closer than R (the fiber radius) from the center of the xy section [9]. Here, the x, y, and z axes coincide with the edges of the cubic lattice. Periodic boundary conditions were assumed at outer simulation box boundaries, resulting in a regular array of straight and parallel fibers ("sample A"). Particle orientations in the fiber surface layer ("ghosts") were fixed in accordance with the desired surface anchoring (here chosen parallel to the fiber direction, z axis) and the corresponding dimensionless anchoring strength was introduced above as $w>0$. The field was applied along the y axis, thereby producing a conflict with the aligning tendency of the polymer network. A similar confinement can be encountered also in crystalline colloids.

We introduce notation in analogy with the switching in a nematic slab where surface anchoring is strong and planar, and a magnetic field is applied along the slab normal. In
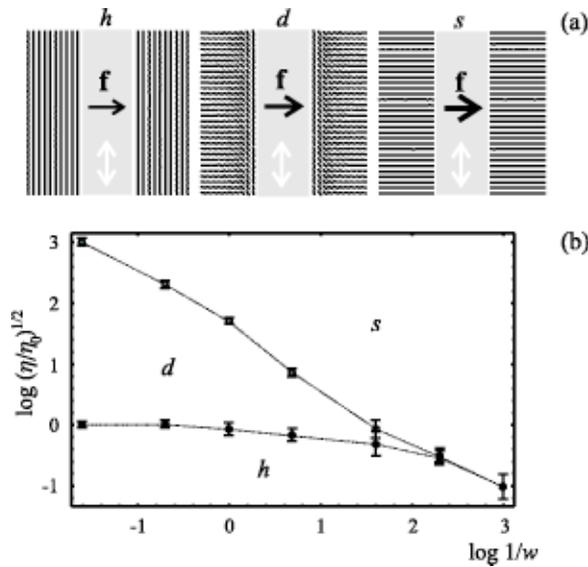
FIG. 1. Structural transitions in sample A. (a) Director fields $\mathbf{n}(\mathbf{r})$ (yz cross sections) for the three possible structures (calculated for $\eta = 0.005$, 0.05, and 0.5; $w = 1$). $\mathbf{n}(\mathbf{r})$ in each point was calculated by diagonalizing the MC cycle-averaged local ordering matrix $Q = \frac{1}{2}(3\langle \mathbf{u}_i \otimes \mathbf{u}_i \rangle - I)$ and identifying the eigenvector corresponding to the eigenvalue with the largest absolute value. (b) The structural phase diagram; η_0 denotes the Fréedericksz threshold for $w = 5$ (strong anchoring).

weak fields the equilibrium director ($\mathbf{n}$) configuration is homogeneous with $\mathbf{n} \perp \mathbf{f}$ ("h structure"). Increasing the field strength, once the Fréedericksz threshold $H_F = \sqrt{k/\chi_a \mu_0}(\pi/\delta)$ is reached, a continuous transition to a deformed structure is observed ("d structure"). Here, k denotes the effective Frank elastic constant, δ the sample thickness, $\chi_a = \chi_{\parallel} - \chi_{\perp}$ the anisotropy of the magnetic susceptibility ($\parallel$ and $\perp$ referring to $\mathbf{n}$), and $\mu_0 = 4\pi \times 10^{-7}$ Vs/Am. For finite anchoring strengths w the threshold H_F is somewhat reduced [13]. Increasing H even further, for finite w the field overwhelms the anchoring, and a second (also continuous) "saturation" transition takes place. Above this second threshold H_s—showing a more significant w dependence than H_F—nematic molecules are aligned uniformly along the field, with $\mathbf{n} \parallel \mathbf{f}$ ("s structure"). Both thresholds, H_F and H_s, have been derived numerically for an arbitrary w in slab geometry, allowing for the construction of a stability phase diagram for the three structures [13]. In case of weak anchoring or in a very thin nematic slab with $k/w \gg \delta$, the thresholds H_F and H_s attain similar values, whereby the stability region for the d structure becomes extremely narrow [13]. There is, however, no triple point in the diagram.

We observe similar structural transitions also in a regular array of polymer fibers, sample A. The yz cross sections of director profiles calculated for each of the three structure types are shown in Fig. 1(a) and the structural phase diagram in Fig. 1(b). Note that for the d structure the nematic is bent in the yz plane, while it is twisted in the xz plane, as opposed to the slab case where the twist deformation is absent. The intermolecular potential (1), however, is spatially isotropic and corresponds to the one-constant approximation in the

Frank elastic description, making thus no distinction in energy for the different deformation modes and causing the switching behavior to be qualitatively close to that observed in slab geometry.

Constructing the diagram, the simulation box size was set to 30^3 particles, which for the chosen fiber radius ($R/a = 5$) amounts to 24600 nematic and 840 ghost particles in total. Then, for each anchoring strength w, the zero-field simulation ($\eta = 0$) started from a completely random orientational configuration, and the Metropolis scheme [14] was employed to update particle orientations [11]. Once the system was equilibrated (after at least 1.2×10^5 MC cycles), a set of further 1.2×10^5 successive cycles was used to calculate relevant observables. In cases with an external field applied ($\eta > 0$), the simulation started from the configuration equilibrated at the next lowest field strength H, thus, performing a "scan" increasing H (and η). For checking, a similar scan was performed also for decreasing η. The order parameter sensitive to field-induced orientational changes was defined as $\langle P_2^f \rangle = \langle \frac{1}{2}[3(\mathbf{u}_i \cdot \mathbf{f})^2 - 1] \rangle$, where the brackets $\langle \cdots \rangle$ represent an average over nematic particles and over MC cycles. The η value yielding the maximum σ^f—the variance of $\langle P_2^f \rangle$ related to collective molecular fluctuations—was used as a reliable enough estimate for the structural transition threshold. Note, however, that if the average $\langle \cdots \rangle$ above is taken over all nematic particles, monitoring σ^f one can detect only the Fréedericksz transition involving a large portion of nematic material. On the other hand, to detect the saturation transition affecting only a few particles near the fiber surface, the average $\langle \cdots \rangle$ is to be calculated exclusively over particles in a thin layer surrounding the fiber (of thickness $\sim a$).

The phase diagram [Fig. 1(b)] was derived for $T^* = k_B T / \epsilon = 1.0$ (recall that the bulk nematic-isotropic transition is observed at $T_{NI}^* = 1.1232$ [11]) and shows stability regions for the h, d, and s director structures. In weak fields one always finds the undistorted h structure, while in strong enough fields the saturated s structure is always seen. The deformed d structure appears at intermediate field strengths, but like in slab geometry its stability region gets narrower upon decreasing w. Due to the low accuracy of threshold estimates for small w, we cannot clearly confirm the absence of the triple point in the diagram. Further, both transitions seem to be continuous: no systematic hysteresis could be detected in external field scans.

In Fig. 1 (b) the Fréedericksz threshold ($h \leftrightarrow d$ line; $\eta_F = 0.0085 \pm 0.0015$ for $w = 1$) indeed decreases with decreasing w, while the saturation threshold ($d \leftrightarrow s$ line; $\eta_s = 0.30 \pm 0.015$ for $w = 1$) shows an even more significant w dependence, approaching $\sqrt{\eta_s} \propto w$ for large w. Similarly as in slab geometry, the position of the $h \leftrightarrow d$ line is expected to strongly depend on the effective fiber-to-fiber distance d_*—with increasing d_* it should move towards lower critical field strengths—while the position of the $d \leftrightarrow s$ line for large enough w should be almost insensitive to changing d_*. These statements were checked in a network consisting of somewhat thinner fibers: setting $R/a = 3$ and considering a smaller sample A with 18^3 particles approximately maintains
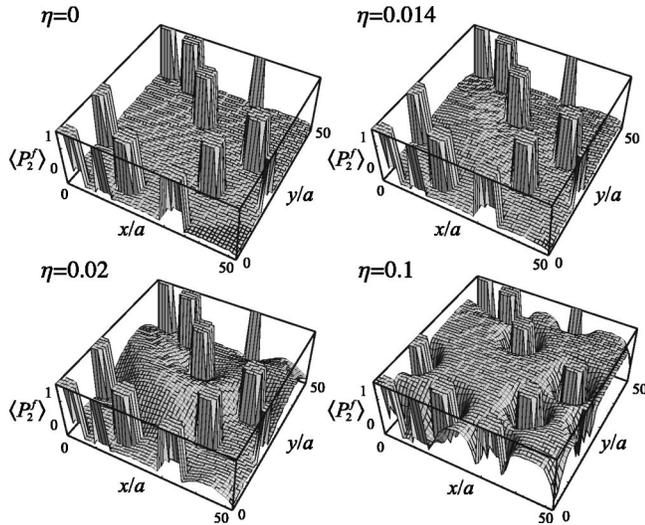
FIG. 2. Array of several straight fibers (sample B): $\langle P_2^f \rangle(\mathbf{r})$ order parameter (xy cross section) for different field strengths (proportional to $\sqrt{\eta}$). "Columns" correspond to fibers.

FIG. 3. Sample C with several distorted fibers: ghost particles fixing the network topography.

the polymer concentration, but decreases the fiber-to-fiber distance from $d_* = 20a$ to $d'_* = 12a$. Having fixed $w = 1$ corresponding to rather strong anchoring with a microscopic extrapolation length k/w (of the order of $\sim a$), the Fréedericksz and saturation thresholds are now found to be $\eta'_F = 0.025 \pm 0.005$ and $\eta'_s = 0.30 \pm 0.03$, respectively. While η_s remained almost unaltered, η_F changed quite significantly, yielding $\sqrt{\eta_F/\eta'_F} \approx 0.58$. This compares well to $d'_*/d_* = 0.6$, which is in agreement with $\sqrt{\eta_F} \propto 1/d_*$ predicted for slab geometry in the strong anchoring limit. Finally, the temperature dependence (in principle) enters the thresholds via k, w, and χ_a (all decrease with increasing T^*). Current preliminary results, however, indicate no dramatic changes in the phase diagram with changing T^*.

A next step towards a more complex polymer network [7,8] was to allow for a distribution of interfiber distances in the system, significantly affecting its switching behavior. We therefore modeled a sample with an irregular array of fibers still straight and parallel (directed along the z axis), yet distributed randomly within the xy plane ("sample B"). Increasing the sample size to 50^3 particles and including eight fibers with $R/a = 3$ and anchoring along the z axis ($w = 1$) again roughly maintains the polymer concentration ($\approx 9\%$). This choice, hence, covers linear length scales of up to ~ 0.25 μm. Again, the external field was applied along the y axis.

Figure 2 shows the evolution of $\langle P_2^f \rangle$ averaged over MC cycles for each particle within a given xy cross section. For $\eta \lesssim 0.013$ one finds $\langle P_2^f \rangle(\mathbf{r})$ negative and almost constant—apart from slight variations close to the fibers attributed to enhanced nematic ordering—showing that particles are still aligned along the z axis and that the Fréedericksz threshold has not been exceeded yet. For $\eta \approx 0.013$—still below the sample A threshold for $R/a = 3$—in polymer-poor regions where the interfiber distance is above average the particle reorientation along $\mathbf{f}$ is initiated and $\langle P_2^f \rangle$ increases, becoming eventually positive. As the field strength is increased
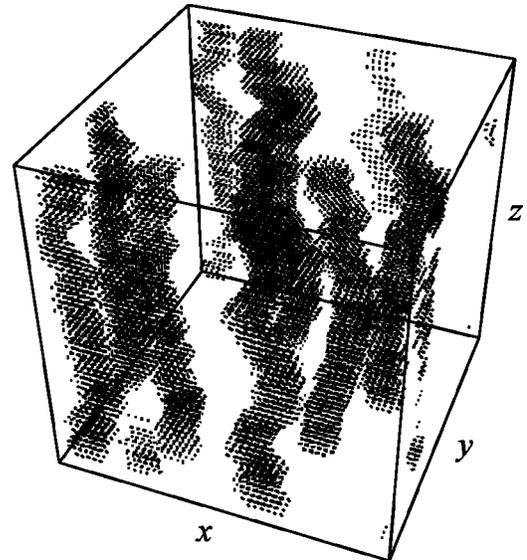
even further, the parallel-to-fiber alignment persists only in polymer-rich regions and near the fibers (see Fig. 2 for $\eta = 0.1$, near the left corner). Finally, for extremely strong fields—far above the saturation transition (e.g., at $\eta = 1$)—all molecules are aligned along $\mathbf{f}$ and, in addition, the bulk degree of nematic order is enhanced. The opposite holds for the fiber vicinity: the degree of order drops below its bulk value due to the conflicting effects of the fibers and external field. Note that unlike the regular sample A the switching in sample B evolved into a rather gradual process.

Finally, dropping the assumption that the fibers be straight and parallel, we considered a system of distorted fibers—Fig. 3, "sample C." Again, the field and average fiber directions were taken along the y and z axes, respectively. Each of the fibers (with uniform cross section, $R/a = 3$) was then generated by performing a biased random walk: while progressing along z, random deviations within the xy plane were performed with a given probability regulating the fiber curvature. Doing this, care was taken to meet the periodic boundary conditions in the z direction. Moreover, everywhere the anchoring easy axis was assumed parallel to the local fiber direction, with $w = 1$. Despite fiber curvature, in absence of external fields ($\eta = 0$) the net molecular orientation is still well defined (along z), except for the fiber vicinity where it is affected by the local anchoring.

For the switching in a symmetry-lacking sample it is instructive to explore simulation-predicted experimental observables, rather than study specific order parameter maps. One of the suitable tools for the monitoring of switching are electric capacitance measurements [8]. They rely on the orientational anisotropy of the molecular dielectric constant, leading to changes in sample capacitance for any major molecular reorientation. These changes will be monitored in the following, along with a detailed comparison of samples A, B, and C. Simulating capacitance, it was assumed that the weak probing electric field is—like the aligning magnetic field $\mathbf{f}$—directed strictly along the y axis throughout the sample,
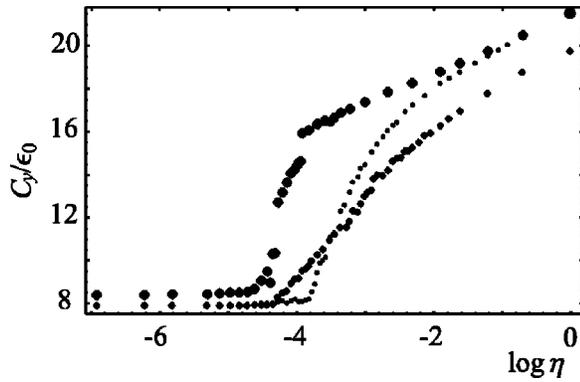
FIG. 4. Switching in LCDNS systems, as monitored via simulated electric capacitance: sample A (small dots), sample B (medium-sized dots), and sample C (large dots).

but is, unlike **f**, not homogeneous. In absence of free ions and provided, moreover, that molecular ordering is mostly restricted to the yz plane and that elastic deformations along z are weak (reasonable for straight or weakly distorted fibers), the effective static capacitance for a M^3 sample can be approximated by [8]

$$C_y = \epsilon_0 \sum_{k=1}^{M} \sum_{l=1}^{M} \left(\sum_{m=1}^{M} \frac{1}{\epsilon(k,l,m)} \right)^{-1}, \qquad (2)$$

where the indices k, l, and m run along the x, z, and y coordinates, respectively. Here, we consider that each group of molecules represented by $\mathbf{u}_i$ and located at (k,l,m) is endowed with a local dielectric constant $\epsilon(k,l,m) = \epsilon_\perp + (\epsilon_\parallel - \epsilon_\perp)(\mathbf{u}_i \cdot \mathbf{f})^2$. Further, $\epsilon_0 \approx 8.85 \times 10^{-12}$ As/Vm.

The calculations were performed for $\epsilon_\parallel = 29.8$ and $\epsilon_\perp = 6.1$, assuming as in Ref. [8] the same dielectric anisotropy for the polymer network. The C_y versus η characteristics for three samples (A, B, and C) with $R/a = 3$ and same polymer concentration ($\approx 9\%$), but different network topography, is

shown in Fig. 4. In Fréedericksz-like geometry, where the external field is strictly perpendicular to fibers (samples A and B), the orientational transition happens abruptly at a well-defined threshold (η_A and η_B, respectively, with $\eta_A > \eta_B$). In sample C network irregularities further decrease the switching threshold (η_C; not well defined anymore), yet keep the reorientational process relatively sudden. The thresholds for the three samples from Fig. 4 can be identified as $\eta_A = 0.022 \pm 0.001$, $\eta_B = 0.013 \pm 0.001$, and $\eta_C = 0.010 \pm 0.002$, with $\eta_C < \eta_B < \eta_A$, as expected. Note that the $C_y(\eta)$ curve is most gradual for sample B because molecules in polymer-rich sample regions refuse to switch unless the field is extremely strong, and that the increase of C_y for large η is to be attributed to enhanced nematic order rather than to particle reorientation.

In summary, we have shown using computer simulations that—contrary to naïve intuition—external field-driven switching in a system of polymer fibers dispersed in nematics is rather sudden even in samples with a fairly disordered fiber arrangement (both positionally and orientationally), and that it appears at a lower threshold, if compared with more regular samples of same polymer concentration. These conclusions were drawn by monitoring the simulated electric capacitance, starting from the simulation data. Moreover, for a regular array of straight and parallel fibers we have simulated a stability phase diagram for possible director structures, indicating a behavior equivalent to that observed in a nematic slab. Our predictions should help to design fiber arrays with controlled disorder that could be prepared by suitably manipulating the excitation light during polymerization [4].

[1] T. Bellini *et al.*, Phys. Rev. Lett. **69**, 788 (1992).
[2] V.G. Nazarenko *et al.*, Phys. Rev. Lett. **87**, 075504 (2001).
[3] G. P. Crawford and S. Žumer, *Liquid Crystals in Complex Geometries Formed by Polymer and Porous Networks* (Taylor and Francis, London, 1996).
[4] R. Penterman *et al.*, Nature (London) **417**, 55 (2002).
[5] I. Dierking *et al.*, Appl. Phys. Lett. **71**, 2454 (1997); Liq. Cryst. **24**, 397 (1998); **24**, 387 (1998).
[6] M.J. Escuti *et al.*, Appl. Phys. Lett. **75**, 3264 (1999).
[7] Y.K. Fung *et al.*, Phys. Rev. E **55**, 1637 (1997).
[8] R.-Q. Ma and D.-K. Yang, Phys. Rev. E **61**, 1567 (2000).
[9] C. Chiccoli *et al.*, Phys. Rev. E **65**, 051703 (2002).
[10] P.A. Lebwohl and G. Lasher, Phys. Rev. A **6**, 426 (1972).
[11] *Advances in the Computer Simulations of Liquid Crystals,* edited by P. Pasini and C. Zannoni (Kluwer, Dordrecht, 2000).
[12] E. Berggren *et al.*, Phys. Rev. E **49**, 614 (1994).
[13] J. Nehring *et al.*, J. Appl. Phys. **47**, 850 (1976).
[14] N. Metropolis *et al.*, J. Chem. Phys. **21**, 1087 (1953).